ISSN 1063-7729, Astronomy Reports, 2012, Vol. 56, No. 2, pp. 146–152. © Pleiades Publishing, Ltd., 2012.
Original Russian Text © V.N. Obridko, V.E. Chertoprud, 2012, published in Astronomicheskii Zhurnal, 2012, Vol. 89, No. 2, pp. 173–179.

Dynamics of the Photospheric Magnetic Field in the Vicinity of the Solar Equator

V. N. Obridko* **and V. E. Chertoprud**

Pushkov Institute of Terrestrial Magnetism, the Ionosphere, and Radio Wave Propagation, RAN, Moscow, Russia

Received July 19, 2011; in final form, August 17, 2011

Abstract—SOHO–MDI daily magnetic field synoptic data (a 14-year series of daily maps of the solar magnetic field intensity B available at the site http://soi.stanford.edu/magnetic/index5.html) have been used to analyze the dynamics of the photospheric magnetic field in the vicinity of the solar equator. The standard deviation s_B of the field B calculated over areas of tens of square degrees on the solar disk was taken as a basic index. An 11-year variation similar to that observed at higher latitudes is observed in the vicinity of the equator, and is similar for weak and strong fields; i.e., the solar cycle exists in the sunspot-free zone. New qualitative data support the idea that the weak background magnetic field increases toward the solar limb. This angular dependence suggests the existence of a transverse component of the background field. The magnetic fields in the vicinity of the equator were significantly different in the initial phases of Cycles 23 and 24. Annual variations of s_B were observed near the center of the solar disk. These variations are due to two factors: the annual variation of the distance from the equator to the disk center and the increase of s_B with with distance from the equator. Reliable detection of these variations is an evidence of high accuracy of the s_B estimates.

DOI: 10.1134/S1063772912010076

1. INTRODUCTION

The analysis of the daily maps of the solar magnetic field B (SOHO/MDI magnetograms) carried out in [1] showed an enhancement of the background magnetic field from the center to the limb of the Sun, which suggested the existence of a significant transverse component of the background field. The re-calibration of the SOHO/MDI data in December 2008 and extension of the observational series necessitated the refinement of the preliminary results using an updated method. The new SOHO/MDI data also provide evidence that the 11-year solar cycle is manifests in the vicinity of the equator (the sunspot-free zone). The solution of these and other related problems essentially reduces to studying the dependence of the background-field parameters on the angle u between the radial and line-of-sight directions for the weak and strong magnetic fields near the equator at different phases of the solar cycle. To obtain these dependences, we analyzed a sequence of daily maps of the solar magnetic field B (MDI 96m Magnetograms, the Lev 1.8.2) covering 192 Carrington rotations (CRs) from May 1996 (CR1908) to July 2010 (CR2099).

*E-mail: obridko@izmiran.ru

2. METHOD

On each map of the solar magnetic field B (with the coordinates x and y), we selected a horizontal rectangular band 951 pixels long (in x) and 101 pixels wide (in y) centered on the central meridian (CM), which was used as a window. Three positions for the window were considered: the center of the band coincident with the map center (C), the southern boundary of the band passing through the map center (N), and the northern boundary of the band passing through the map center (S). All bands were located in the vicinity of the equator at the mean latitudes $\pm 6°$ (C), 0–12°N (N), and 0–12°S (S). These latitude zones could spread by $\pm 7°$ due to annual variations in the distance from the equator to the center of the Sun. Each window was divided into 19 rectangular sections of 50×101 pixels.

In each section, we determined the mean field $\langle B \rangle$, the mean field modulus $\langle |B| \rangle$, the mean square $\langle B^2 \rangle$, the dispersion $D = \langle B^2 \rangle - \langle B \rangle^2$, and the standard deviation $s_B = D^{1/2}$ for all field values in a given range $B_1 < |B| \leq B_2$, as well as the asymmetry and excess coefficients. At this stage of the analysis, we focused on one parameter—s_B. Note that, near the solar equator, $\langle B^2 \rangle \gg \langle B \rangle^2$ at virtually all times, so that the difference between the temporal (or spatial)

variations of $\langle B^2\rangle^{1/2}$ and s_B is insignificant; i.e., the choice between s_B and $\langle B^2\rangle^{1/2}$ (or even $\langle B^2\rangle$) is not critical when considering such variations. However, estimates of $\langle B^2\rangle$ are directly associated with the magnetic field energy, while estimates of D (or s_B) are independent of any errors in the field zero reading.

The variations of s_B (or other parameters) in different intensity ranges differ significantly in amplitude. For convenience, the data are sometimes represented in a standardized form: $x \to x_s = [x - m(x)]/s(x)$, where $m(x)$ and $s(x)$ are the mean and standard deviation of x, respectively, on the curve considered.

Calculations were performed imposing different restrictions on $|B|$ (in particular, $|B| \le 75$ G, $|B| > 75$ G, and 75 G $< |B| <$ 400 G). The daily parameters obtained were averaged over each Carrington rotation. Thus, we eliminated effects associated with longitudinal variations of the magnetic-field parameters.

By considering the results obtained for different rectangular sections, we could determine the dependence of the magnetic-field parameters on the angle u between the normal and the direction to the observer. In the middle (central) sections, this angle is close to zero, while it can reach 70° in the lateral sections. The angle u was measured such that, in the equatorial region, it was positive at eastern longitudes (i.e., to the left of the CM) and negative at western longitudes. The analysis of the calculations with different restrictions on $|B|$ demonstrates the characteristics of the angular dependence for weak and strong fields.

The differences between these calculations and those performed in [1] are as follows.

(1) The windows chosen here are located only in the equatorial zone.

(2) The window sections for estimating the parameters have been changed.

(3) We are using daily magnetograms recalibrated in December 2008.

(4) The time interval for the observation series has been extended by 3.5 years.

(5) Instead of the 22 monthly observational series at approximately half-year intervals analyzed in [1], we use here a series of 192 CRs nearly without gaps (i.e., the data volume has increased by a factor of eight).

(6) Data obtained for the standard orientation of the SOHO camera have been analyzed and compared with those obtained with the camera rotated by 180°.

(7) The basic parameter analyzed here is s_B instead of the parameter $\langle B^2\rangle$ considered in [1].

3. RESULTS

Our analysis of a 14-year series of daily solar magnetic maps (the recalibrated SOHO/MDI magnetograms) confirms the center-to-limb effect in the distribution of the magnetic-field intensity found in [1]. Note that here, as distinct from [1], we are only considering this effect in the vicinity of the equator, so that we eliminate the influence of latitude variations of the magnetic-field parameters.

Recall that the magnetograph measures the longitudinal (line-of-sight) component of the magnetic field. The relationship between the longitudinal and transverse (across the line-of-sight) components can be specified by analyzing the center-to-limb variation.

The main effect manifest in the distribution of $sB(u)$ is the increase of s_B for weak fields and decrease for strong fields with increasing $|u|$. This confirmss an important property of the solar magnetic fields—the existence of two field subsystems. The stronger fields are mainly radial, and their departure from the normal begins higher above the photosphere. This hypothesis was adopted as a basis for the new method of calculating the coronal magnetic field [2, 3].

Since regular magnetographic measurements of photospheric magnetic fields were started, various models have been proposed for calculating magnetic fields at specified altitudes above the photosphere. The first (in the late 1970s) was the well-known and now widely used potential-field model—the source surface, whose radius was taken to be 2.5 $R_\odot$. Since the magnetograph measures the line-of-sight magnetic field and the boundary condition is the known the radial component, an additional assumption concerning the photospheric field is necessary. It was naturally suggested that the potentiality condition also holds at a photospheric boundary surface. One can then calculate the longitudinal component with undefined coefficients and find the full solution of the problem through comparisons with observations. This was realized in the papers cited above. However, Svalgaard et al. [4] analysis of Stanford magnetograms showed that the dependence of the signal on the observation point on the disk acted as if the magnetic field were strictly vertical over a long distance. In fact, the potential approximation assumes an absence of currents in the medium. Obviously, this is not quite correct as far as the photosphere is concerned. Stenflo and Fogel [5] later showed that the concept of kilogauss flux tubes combined with increased buoyancy of these tubes should also lead to an enhancement of the vertical component of the photospheric magnetic field. In the model that is most frequently used for such field calculations at

high altitudes [2, 3], the photospheric magnetic field is vertical, in accordance with the results of Svalgaard et al. [4], and the source surface is assumed to be at 3.25 $R_\odot$.

Since the strong photospheric fields are radial, the line-of-sight (longitudinal) component decreases when observed at the limb. This is the standard center-to-limb effect (Fig. 1).

On the other hand, recent observations with high-resolution magnetographs have provided evidence that the small-scale field may instead be horizontal. Some evidence for this was provided by the first measurements with vector magnetographs [6]. The fields observed in the vicinities of active centers were complex and mainly transverse. However, not until the launch of the Hinode satellite could the existence of strong transverse fields in the unperturbed or only weakly perturbed photosphere be confirmed directly [7].

This result was obtained independently in [1] from the analysis of daily intensity maps of the solar magnetic field B (SOHO/MDI magnetograms). The weak fields demonstrated a completely different type of behavior than the strong field. While the strong fields display the "normal" center-to-limb effect (i.e., the signal decreases towards the limb, as it should in a mainly radial field), the weak background fields display an increase towards the limb. This can be called an "inverse" center-to-limb effect. It is characteristic of a mainly transverse "divergent" magnetic field. We have confirmed this effect using a much more extensive database here (see Fig. 2).

A weak field of the order of 1–2 G that nearly doubled towards the limb was revealed from by analysis of SOLIS and GONG observations in [8], where this effect was interpreted as a result of mainly horizontal fields in the quiet Sun. In addition, these fields changed rapidly on characteristic time scales of the order of tens of minutes.

The recent analysis of Hinode data in [9, 10] shows that small-scale transverse magnetic fields contribute significantly to the observed background field. On the whole, this agrees with our results. Thus, small-scale, background, relatively weak magnetic fields seem to form a specific population governed by its own cyclic laws.

The center-to-limb effect for strong fields in the vicinity of the equator consists of a decrease of s_B towards the limb. The higher the value of $sB(u)$, the steeper the decrease. We can also see an 11-year periodicity. The center-to-limb effect for the weak equatorial fields consists of an increase of s_B towards the limb, likewise with an appreciable 11-year periodicity.

Both the normal and the inverse center-to-limb effects are manifest similarly in each of the three latitude bands considered (C, N, S), and are qualitatively preserved in different time periods, at different phases of the 11-year cycle, and for changing differences between the strong and weak fields from 50 to 100 G. However, some parameters of this effect change in time.

These two circumstances—the opposite variations of $sB(u)$ for weak and strong fields and the change of the amplitude of the $sB(u)$ variations with the phase of the cycle—make it impossible to account for or eliminate the center-to-limb effect by choosing a proper calibration.

On the whole, after standardization, both populations display the same dependence on the phase of the cycle (see Fig. 3)

The curves for the longitudinal dependence of the weak fields at different phases of the cycle do not differ significantly. The curves for the beginnings of Cycles 23 and 24 essentially coincide. The curves for strong fields are also similar at all phases.

However, there is one important difference, which shows that the behavior of the weak and strong fields is not fully identical at different phases of the cycle. While the amplitudes of the weak fields are approximately equal at the beginning of Cycles 23 and 24, the strong fields display a clear difference, which is visible in Fig. 3 and becomes even more obvious in Fig. 4. It turned out unexpectedly that the value of $sB(u)$ for the strong fields was much higher at the beginning of Cycle 24 than at the beginning of Cycle 23 (see Fig. 3). This is at variance with the behavior of the sunspot numbers, which were much higher in the first period (1996–1999, annual mean sunspot numbers of 8.6, 21.5, 64.3, and 99.3) than in the second period (2006–2010, annual mean sunspot numbers of 15.2, 7.5, 2.9, 3.1, and 16.7).

This may be a result of nonstandard behavior of Cycle 23, when the declining phase was unusually long and the rise phase did not actually begin until 2009–2010. Therefore, in calculating the center-to-limb variations represented in Fig. 4, the decline of Cycle 23 and the beginning of Cycle 24 were particularly well separated. Even so, curve 4 for the beginning of Cycle 24 (2008.12–2010.07) passed much higher than curve 1 for the beginning of Cycle 23 (1996.05–1997.11).

On the other hand, curves *3* and *4* pass very close to one another; i.e., the formal end of Cycle 23 and the beginning of Cycle 24 in December 2008 did not affect the strong magnetic fields. This means that the boundary between Cycles 23 and 24 is not unusual. The same is true for the weak fields, which

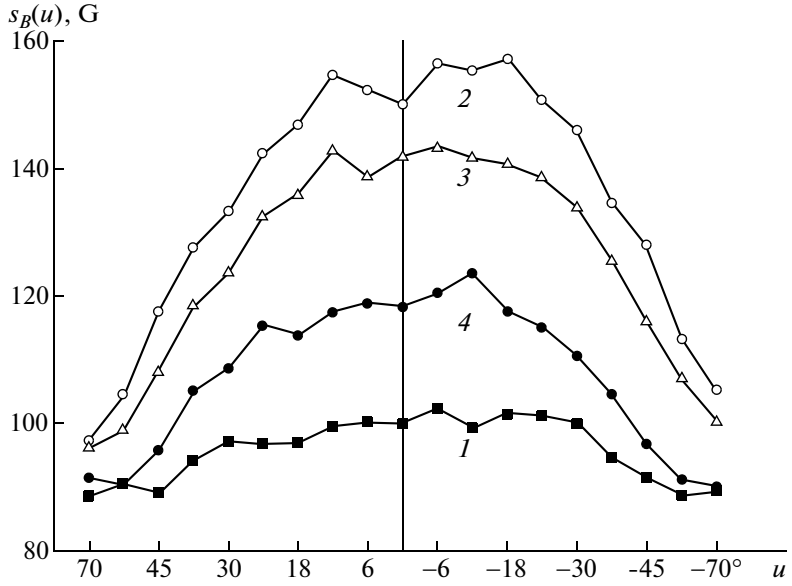

Fig. 1. The dependence $sB(u)$ at the latitudes $\phi \simeq \pm 6°$ for $|B| > 75$ G. Four observation intervals are illustrated: (*1*) 1908–1954CR (1996–1999); (*2*) 1955–1995CR (1999–2002); (*3*) 1996–2042CR (2002—2006); and (*4*) 2043–2099CR (2006–2010). The camera was operated in the normal (standard) mode; i.e., the angle P between the upward direction on the magnetic map and the northward direction was zero.

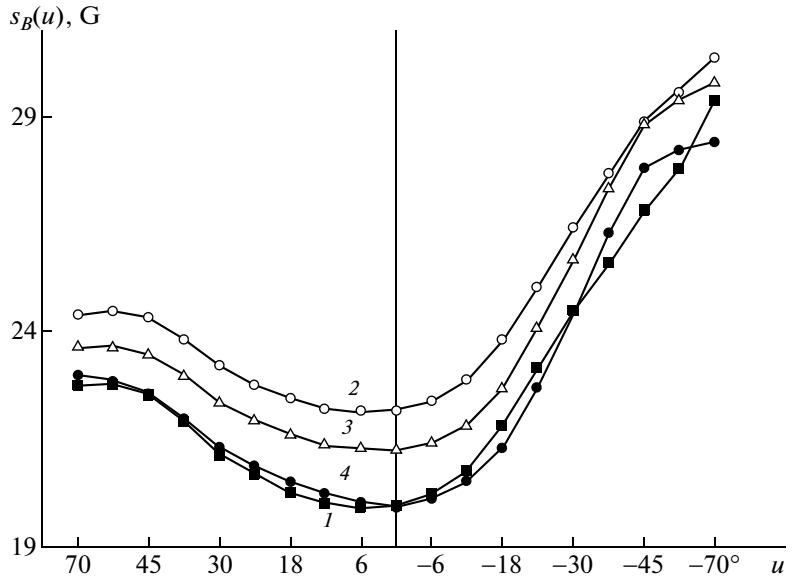

Fig. 2. The dependence $s_B(u)$ at the latitudes $\phi \simeq \pm 6°$ for $|B| \leq 75$ G for the same time intervals as in Fig. 1 at $P = 0$.

were in no way affected by passing through the minimum. Nor were there any significant deviations from the 11-year cycle in 2003, when the reversal of the zonal component of the equatorial magnetic field could be inferred from the Stanford WSO data (http://wso.stanford.edu/gifs/all.gif).

In Figs. 1 and 2, we can see an East–West asymmetry in the distribution of $s_B(u)$, which is due to cell-to-cell variations of the noise level in the camera. This was established by comparing the $s_B(u)$ curves for 2006–2010 obtained with the standard orientation of the camera and with the camera rotated by 180° (the difference between the compared curves changes sign when moving from East to West). Figure 5 illustrates the $s_B(u)$ variations for the standard orientation of the camera ($s_B(u)_1$, curve *1*) and with the camera rotated by 180°, with subsequent recovery of the East–West direction ($s_B(u)_2$, curve *2*).

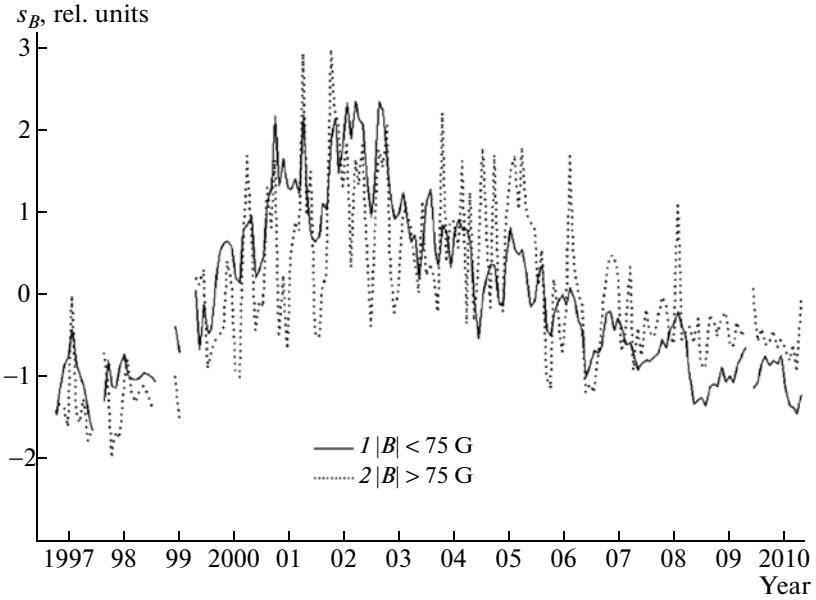

Fig. 3. The 11-year variation of s_B at the latitudes $\phi \simeq \pm 6^\circ$ for $|B| \leq 75$ G (*1*) and $|B| > 75$ G (*2*) at $P = 0$.

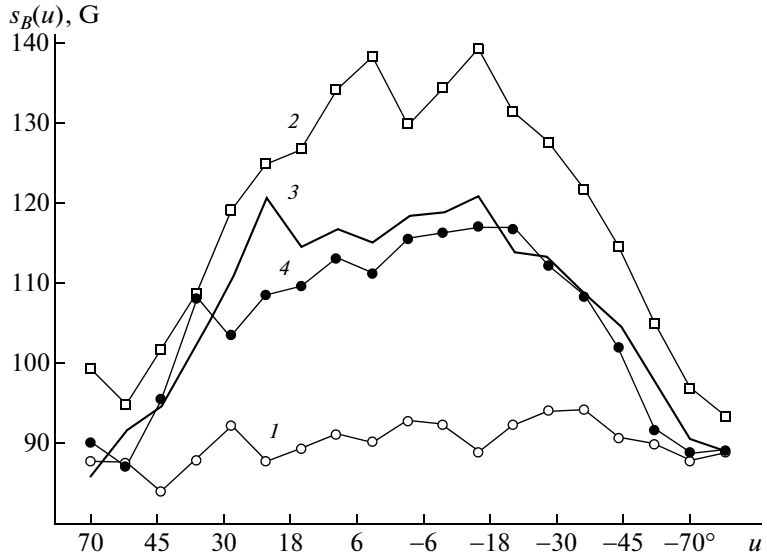

Fig. 4. The dependence $s_B(u)$ at the latitudes $\phi \simeq \pm 6^\circ$ for 75 G $< |B| <$ 400 G, and $P = 0$, at (*1*) the beginning of Cycle 23 (1908–1929CR $\sim$ 96.05–97.11), (*2*) the decline of Cycle 23 (2037–2058CR $\sim$ 05.11–07.06), (*3*) the end of Cycle 23 (2059–2077CR $\sim$ 07.07–08.12), and (*4*) the beginning of Cycle 24 (2078–2099CR $\sim$ 08.12–10.07).

The difference between curves *1* and *2* changes sign from minus to plus when moving from East to West. As this takes place, $|s_B(u)_1 - s_B(-u)_1| \simeq |s_B(u)_2 - s_B(-u)_2|$, which indicates an increased noise level in the right part of the camera in the vicinity of the equator. The noise non-uniformity is smoothed out in the mean curve, $s_B(u)_3 = (s_B(u)_1 + s_B(u)_2)/2$ (curve *3*).

During the first eight years of the mission, the camera did not "turn somersaults," and the data for this period were used to determine the annual variations of s_B in two narrow latitude bands (0–12N and 0–12S). Annual variations of s_B were detected on the central meridian. These are due to two factors: the annual variation of the distance from the equator to the disk center and the increase of s_B with distance from the equator. The fact that these variations are reliably detected confirms the high accuracy of the s_B estimates (Fig. 6).

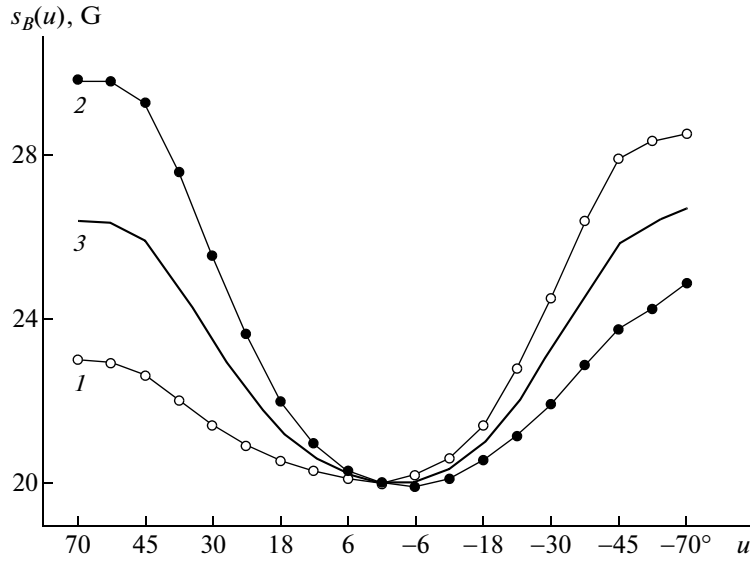

Fig. 5. The dependence $s_B(u)$ at the latitudes $\varphi \simeq \pm 6°$ for $|B| \leq 75$ G with (*1*) the camera operated in the normal (standard) mode and (*2*) the camera rotated by ∼180° (i.e., at $|P| \sim 180°$). The observation interval is 2037–2097CR. Curve *2* was plotted with allowance for the image rotation angle. The mean dependence (*3*) was also plotted using the data (*1*) and (*2*).

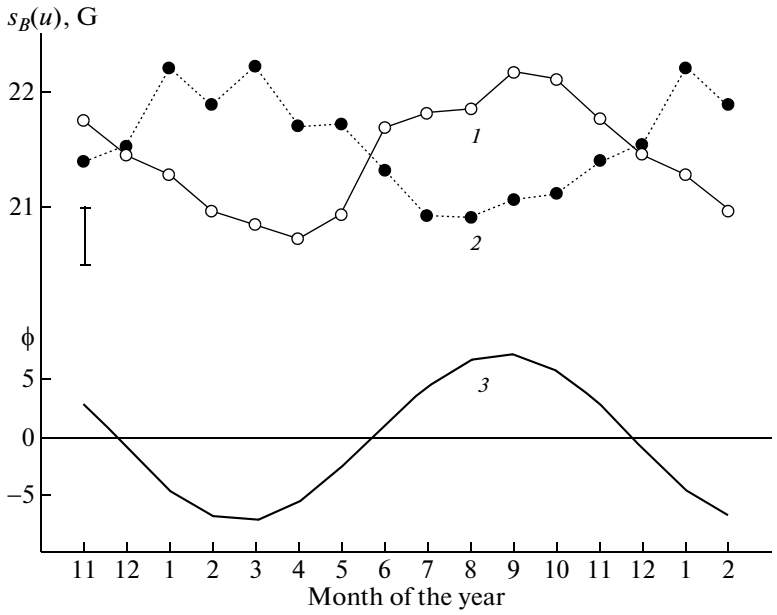

Fig. 6. The annual variation of s_B in two narrow latitude bands 0–12N (*1*) and 0–12S (*2*) for $|B| \leq 75$ G and variation of the heliographic latitude φ of the disk center (*3*). The observation interval is 97 solar rotations, $P = 0$.

4. CONCLUSION

Our study has confirmed that the weak and strong magnetic fields in the equatorial region form two populations that differ markedly in the prevalent direction of the field. The stronger fields are normal to the solar surface and are characterized by positive center-to-limb variations. The weaker fields are mainly tangential and display the opposite center-to-limb effect. 11-year variations of the sort observed at higher latitudes that are manifest in the same way for weak and strong fields were detected in the vicinity of the equator; i.e., the solar cycle is manifest in the sunspot-free zone. However, although they have the same period, the cyclic variations of the weak and strong fields at a given phase of the solar cycle differ. The weak fields behaved similarly at the minima of Cycles 23 and 24, while the strong fields are much stronger at the beginning of Cycle 24 than at the

beginning of Cycle 23. This is in contrast to the corresponding behavior of sunspots.

ACKNOWLEDGMENTS

We are grateful to the SOHO/MDI team for the data provided. This work was supported by the Russian Foundation for Basic Research (projects 11-02-00259 and 10-02-00960).

REFERENCES

1. B. A. Ioshpa, V. N. Obridko, and V. E. Chertoprud, Astron. Lett. **36**, 424 (2009).
2. Y. M. Wang and N. R. Sheeley, Astrophys. J. **392**, 310 (1992).
3. Y. M. Wang and N. R. Sheeley, Geophys. Res. Lett. **27**, 505 (2000).
4. L. Svalgaard, T. L. Duvall, Jr., and P. M. Scherrer, Solar Phys. **58**, 225 (1978).
5. J. O. Stenflo and M. Vogel, Nature **319**, 285 (1986).
6. B. A. Ioshpa and V. N. Obridko, Sov. Astron. **7**, 776 (1963).
7. B. Lites, M. Kubo, H. Socas-Navarro, et al., Astrophys. J. **672**, 1237 (2008).
8. J. W. Harvey, D. Branston, C. J. Henney, and C. U. Keller, Astrophys. J. **659**, L177 (2007).
9. R. Ishikawa, S. Tsuneta, K. Ichimoto, et al., Astron. Astrophys. **481**, L25 (2008).
10. M. Schüssler and A. Vögler, Astron. Astrophys. **481**, L5 (2008).

Translated by V. Obridko